# Cyclotetrabenzil-Based Porous Organic Polymers with High Carbon Dioxide Affinity

Timur Ashirov[a] 🄳
Maymounah Alrayyani[b,c] 🄳
Kyung-Seob Song[a]
Ognjen Š. Miljanić*[c] 🄳
Ali Coskun*[a] 🄳

[a] Department of Chemistry, University of Fribourg, Chemin du Musee 9, 1700, Fribourg, Switzerland
[b] Chemistry Department, Faculty of Science, King Abdulaziz University, Jeddah 23218, Saudi Arabia
[c] Department of Chemistry, University of Houston, 3585 Cullen Boulevard #112, Houston, TX 77204-5003, United States
miljanic@uh.edu; ali.coskun@unifr.ch
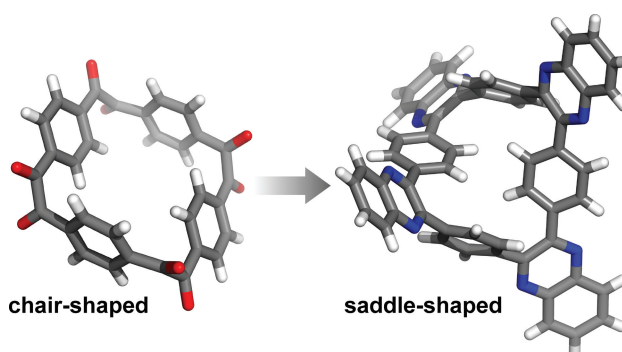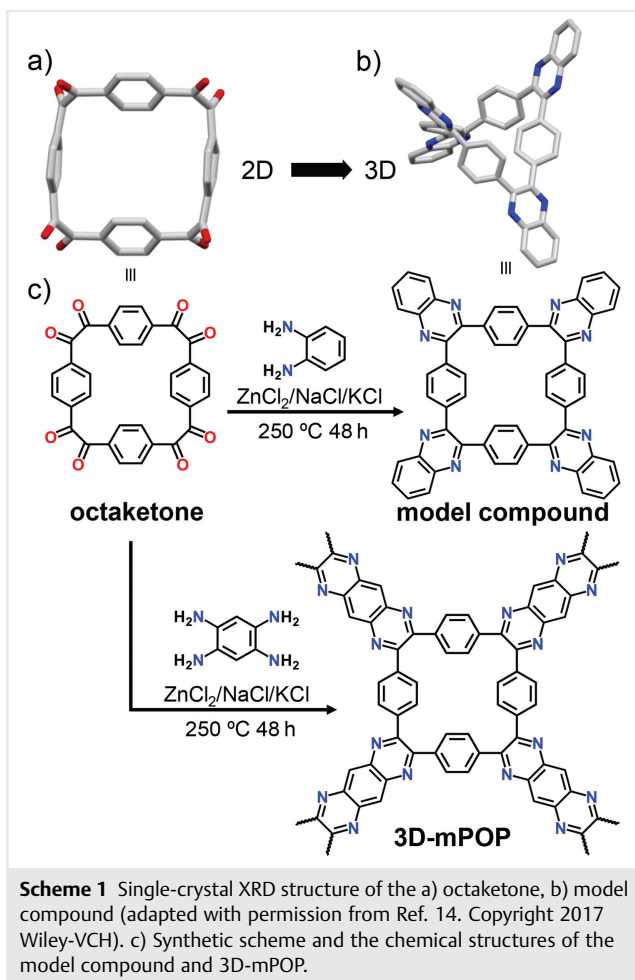
chair-shaped → saddle-shaped

Abstract Porous organic polymers (POPs) incorporating macrocyclic units have been investigated in recent years in an effort to transfer macrocycles' intrinsic host–guest properties onto the porous networks to achieve complex separations. In this regard, highly interesting building blocks are presented by the family of cyclotetrabenzoin macrocycles with rigid, well-defined, electron-deficient cavities. This macrocycle shows high affinity towards linear guest molecules such as carbon dioxide, thus offering an ideal building block for the synthesis of CO_2-philic POPs. Herein, we report the synthesis of a POP through the condensation reaction between cyclotetrabenzil and 1,2,4,5-tetraaminobenzene under ionothermal conditions using the eutectic zinc chloride/sodium chloride/potassium chloride salt mixture at 250 °C. Notably, following the condensation reaction, the macrocycle favors three-dimensional (3D) growth rather than a two-dimensional one while retaining the cavity. The resulting polymer, named 3D-mPOP, showed a highly microporous structure with a BET surface area of 1142 $m^2\,g^{-1}$ and a high carbon dioxide affinity with a binding enthalpy of 39 $kJ\,mol^{-1}$. Moreover, 3D-mPOP showed very high selectivity for carbon dioxide in carbon dioxide/methane and carbon dioxide/nitrogen mixtures.

Key words macrocycles, porous polymers, host–guest chemistry, ionothermal synthesis, CO_2 capture

Introduction

The environmental impact of greenhouse gas emissions is an ever-growing concern, primarily due to the continuously rising atmospheric levels of carbon dioxide (CO_2), which have surpassed 400 ppm.[1] In addition to lowering the world's reliance on fossil fuel energy,[2] technologies to capture CO_2 will be needed to minimize the environmental impact of this gas. In this regard, porous materials have gained tremendous attention. Light-weight porous organic polymers (POPs) with high surface areas, structural tunability, chemical stability, scalability and ease of preparation are intriguing candidates to tackle this problem.[3] The CO_2 affinity of a POP is determined by two main parameters: (a) the size of the pores, which should be in the ultramicropore (~0.7 nm) to micropore range (<2 nm) and (b) the presence of heteroatoms such as nitrogen that can enhance dipole–quadrupole interactions with CO_2.[4] Shape-persistent macrocycles and cages can offer well-defined binding sites for CO_2 molecules and facilitate its efficient capture and separation.[5] In this direction, POPs containing macrocycle or cage-building blocks have gained significant interest in recent years and have already found applications in water/air purification,[6] natural gas purification,[3d,7] adsorption of toxic pollutants[8] and as battery electrodes.[9] The macrocycles including cyclodextrins, calix[4]arenes, resorarenes, and pillar[5]arenes have already been integrated into the POPs.[10] Recently, Miljanić and coworkers reported a facile and a scalable approach for the preparation of cyclotetrabenzoin macrocycles and their esters.[11] Cyclotetrabenzoin esters feature a well-defined, electron-deficient cavity, which is shown to be selective towards linear guest molecules such as terminal alkynes, organic nitriles,[12] CS_2, and CO_2,[13] and a surface area greater than 500 $m^2\,g^{-1}$ in the case of cyclotetrabenzoin acetate. It has also been reported that larger guests such as benzonitrile and phenyl acetylene do not fit in the cavity.[12] The oxidation of cyclotetrabenzoin to the corresponding octaketone dubbed cyclotetrabenzil (labeled as *octaketone* in Scheme 1a) enabled further derivatization through a condensation reaction with 1,2-phenylenediamines to form pyrazine linkages. Interestingly, whereas the acetylated

Scheme 1 Single-crystal XRD structure of the a) octaketone, b) model compound (adapted with permission from Ref. 14. Copyright 2017 Wiley-VCH). c) Synthetic scheme and the chemical structures of the model compound and 3D-mPOP.

cyclotetrabenzoin largely retains the square-grid structure of the parent cyclotetrabenzoin, steric hindrance generated by pyrazine linkages forced the macrocycle to adopt a saddle-shaped three-dimensional (3D) structure, with pyrazine linkages arranged in an alternating manner, thus offering a unique platform for the synthesis of fully sp²-hybridized 3D-POPs.[15]

Results and Discussion

The cyclotetrabenzoin itself is highly insoluble due to the strong intermolecular hydrogen bonding interactions.[15b] Upon its treatment with nitric acid, it is oxidized to the corresponding cyclotetrabenzil octaketone, which has a much higher solubility as it is no longer a hydrogen bond donor.[14] The X-ray diffraction (XRD) crystal structure of octaketone shows a geometry that resembles a chair. One pair of rings is facing each other, with an interplanar distance of 7.64 Å, while the other pair finds themselves in parallel planes (interplanar distance: 4.23 Å) but offset from

each other. The neighboring carbonyl groups are almost perpendicular to each other, with O=C–C=O dihedral angles of 82.1° and 88.3°. In the extended packing diagram of this compound, noticeable are short (2.34 Å) contacts between carbonyl oxygens on one molecule and aromatic hydrogens on the neighboring molecule. The condensation reaction between octaketone and 1,2-phenylenediamine in ethanol affords the corresponding pyrazine-functionalized model compound, whose structure is highly distorted into a 3D structure resembling a saddle, as evidenced from the single-crystal X-ray structure. Within the central macrocycle, one pair of aromatic planes is almost parallel (7.2° interplanar angle), while the other shows significant twisting with an interplanar angle of 80.6°. The planes of the appended quinoxaline moieties on the opposite sides of this model compounds form a V-shape with interplanar angles of 69.7° and 73.8°.

There are only a handful of fully sp²-hybridized organic linkers (such as e.g. cyclooctatetraene), which are at the same time synthetically accessible and deplanarized enough to offer a 3D arrangement, though none of these linkers features an intrinsic pore. Inspired by these results, we targeted the synthesis of a macrocycle-containing 3D POP, 3D-mPOP, by reacting octaketone with 1,2,4,5-tetraaminobenzene under ionothermal conditions using a ZnCl₂/KCl/NaCl eutectic salt mixture (Scheme 1c) at 250 °C.[16] Since the eutectic salt mixture has a lower melting point than ZnCl₂, it enables the polymerization reaction to proceed at lower temperatures, which is critical to avoid partial carbonization. The formation of 3D-mPOP was verified by Fourier-transform infrared (FTIR) and X-ray photoelectron spectroscopy (XPS) analyses (Figure 1a, b). FTIR spectra revealed the formation of pyrazine linkages as evidenced by the C=N stretching band at 1669 cm⁻¹. We also observed a residual C=O stretching at 1696 cm⁻¹.[17] The –NH₃⁺ stretching band of 1,2,4,5-tetraaminobenzene tetrahydrochloride (TABH) at 2466 cm⁻¹ also disappeared, further indicating the successful formation of pyrazine linkages. We also observed the characteristic aromatic =C–H stretching and bending modes at 3000 and 1413 cm⁻¹, respectively (Figure 1a). The XPS N1s spectrum revealed the –C–N– and –C=N– peaks at 398.8 and 400.2 eV, respectively, which were in a perfect agreement with those of pyrazine moieties.[18] Moreover, the C 1s spectrum revealed three different carbon binding energies at 284.5, 285.5 and 286.8 eV, representing the characteristic –C–C–/–C=C–, –C–N–, and –C=N–signatures, respectively (Figure 1b).[19] As a control sample, the model compound was synthesized under the same reaction conditions by reacting octaketone with 1,2-diaminobenzene in an 85% yield (see Figure S1 for the characterization data).[14] The powder XRD analysis of the 3D-mPOP revealed its amorphous nature (Figure S2). In addition, the chemical structure of the 3D-mPOP was verified by solid-state cross-polarization magic-angle

348

Organic Materials   T. Ashirov et al.   THIEME OPEN ACCESS   **Original Article**
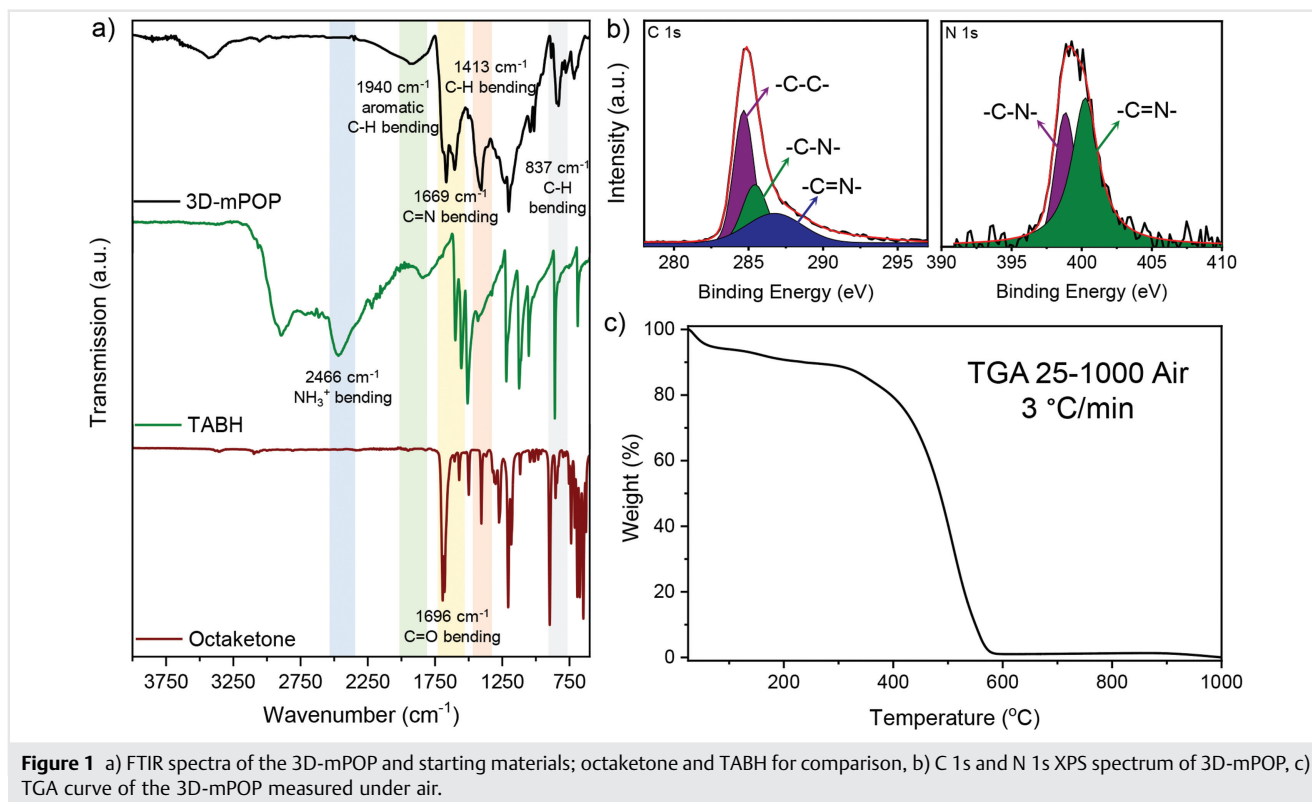
Figure 1 a) FTIR spectra of the 3D-mPOP and starting materials; octaketone and TABH for comparison, b) C 1s and N 1s XPS spectrum of 3D-mPOP, c) TGA curve of the 3D-mPOP measured under air.

spinning ^{13}C NMR analysis. The solid-state ^{13}C NMR spectrum of 3D-mPOP is (Figure S3) found to be in good agreement with that of the model compound. In line with the FTIR data, we observed the presence of terminal carbonyl moieties at 194 ppm. Elemental analysis (EA) was performed to determine the elemental composition of 3D-mPOP (Table S1). The EA data showed 76.7% of C, 14.8% of N and 5.2% of H, in good agreement with the calculated data. We attributed the slight deviation in the C and N contents to the presence of water molecules trapped within the pores, as verified by the presence of a broad peak at 3300 cm^{-1} in the FTIR spectrum (Figure 1a). Thermogravimetric analysis (TGA) data showed that the synthesized polymer is stable up to 350 °C under both air (Figure 1c) and N_2 (Figure S4) atmosphere. The initial mass loss is attributed to the removal of trapped solvents and water. Complete removal of the salts can be verified by TGA under air where 100% mass loss is obtained at 1000 °C (Figure 1c).

The porosity and pore structure of 3D-mPOP and the model compound were analyzed with N_2 sorption measurements at 77 K (Figure 2a). The surface area was calculated from adsorption isotherms using the Brunauer–Emmett–Teller (BET) theory[20] and the pressure ranges were determined from the Rouquerol plots (Figure S5). 3D-mPOP showed a Type I isotherm showing a highly microporous structure. On the contrary, the model com-

pound showed a Type III adsorption isotherm indicating a nonporous or macroporous structure (Figure 2a). While 3D-mPOP has a BET surface area of 1142 m^2 g^{-1}, that of the model compound was found to be only 31 m^2 g^{-1} (Figure 2a and Table 1). The scanning electron micrographs (SEMs) revealed an interconnected pore structure presumably due to the templating effect of the salts[16,21] (Figure S6). The nonlocal density functional theory (NLDFT) pore size distribution analysis showed the presence of two types of micropores with respective sizes of 5.4 and 11.4 Å (Figure 2b). The 5.4 Å-sized pore corresponds to the center of the distorted pyrazine-based macrocycle cavity and the 11.4 Å-sized pore corresponds to the extrinsic pores formed after the polymerization. The H4 hysteresis in the desorption branch at $P/P_0 = 0.4$ points to the presence of mesopores and a slit-like pore structure.[22]

The microporous structure of 3D-mPOP was further examined by CO_2, CH_4, and N_2 uptake (Figure 2c) experiments. The CO_2 gas uptake at 273 K was found to be 2.29 mmol g^{-1}, followed by 0.51 mmol g^{-1} for CH_4, and almost no uptake of N_2 (0.14 mmol g^{-1}). These results clearly demonstrate (Table 2) the CO_2-philicity of the 3D-mPOP, which is likely arising from the cyclotetrabenzoin macrocycle, which was shown to be a good host for the various linear molecules including CO_2.[11,13] The isosteric heat of adsorption (Q_{st}) for CO_2 was calculated from the

349

Organic Materials   T. Ashirov et al.   THIEME OPEN ACCESS   **Original Article**
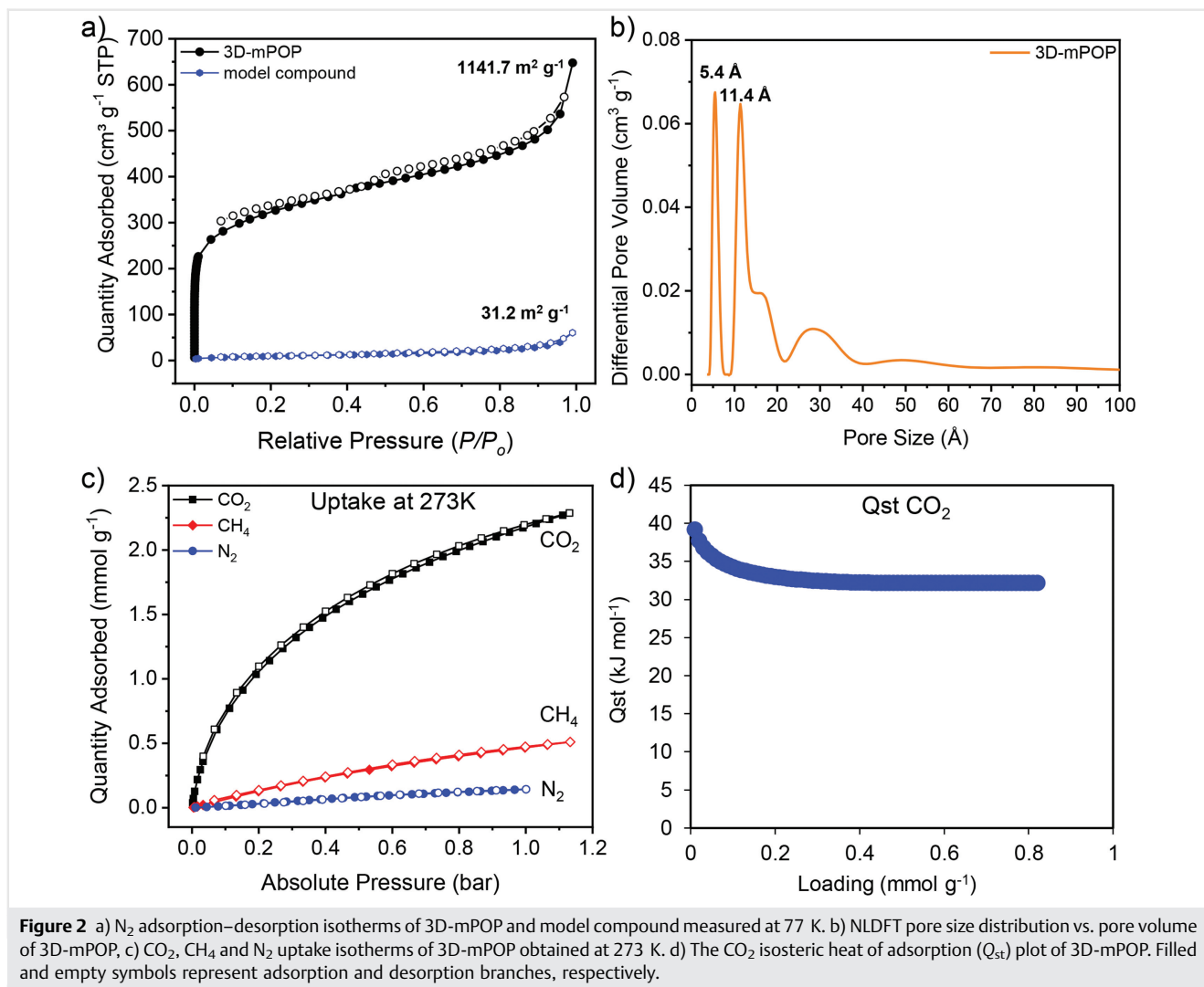
Figure 2 a) N_2 adsorption–desorption isotherms of 3D-mPOP and model compound measured at 77 K. b) NLDFT pore size distribution vs. pore volume of 3D-mPOP, c) CO_2, CH_4 and N_2 uptake isotherms of 3D-mPOP obtained at 273 K. d) The CO_2 isosteric heat of adsorption (Q_{st}) plot of 3D-mPOP. Filled and empty symbols represent adsorption and desorption branches, respectively.

Table 1 N_2 adsorption–desorption analysis results of the model compound and 3D-mPOP at 77 K

Sample	BET[a] ($m^2\ g^{-1}$)	S_{micro}[b] ($m^2\ g^{-1}$)	S_{ext}[c] ($m^2\ g^{-1}$)	V_{total}[d] ($cm^3\ g^{-1}$)	V_{micro}[e] ($cm^3\ g^{-1}$)	V_{ext}[f] ($cm^3\ g^{-1}$)
Model compound	31	–	–	–	–	–
3D-mPOP	1142	561	581	1.00	0.24	0.76

[a]BET surface area calculated over the pressure range (P/P_0) of $0.01 - 0.11$.
[b]Micropore surface area calculated using the t-plot method.
[c]$S_{ext} = S_{total} - S_{micro}$.
[d]Total pore volume obtained at $P/P_0 = 0.99$.
[e]Micropore volume calculated using the t-plot method.
[f]$V_{ext} = V_{total} - V_{micro}$.

adsorption isotherms obtained at 273, 298, and 323 K (Figure S7).[3e] The Q_{st} value for CO_2 was found to be in the range of 32.2–39.2 kJ mol^{-1} (Figure 2d), Notably, the Q_{st} value of 39.2 kJ mol^{-1} at zero coverage clearly shows that

the affinity of the 3D-mPOP towards CO_2 is dictated by the macrocyclic units.[3] Moreover, the calculated Q_{st} value is highly favorable as the adsorption is physical, which results in easier regeneration.[3e] Given the high affinity of 3D-mPOP

Table 2 CO_2, CH_4 and N_2 uptake capacities of 3D-mPOP along with the corresponding isosteric heats of adsorption (Q_{st}) and IAST CO_2/gas selectivities

	CO_2 uptake (mmol g^{-1})				CH_4 uptake (mmol g^{-1})	N_2 uptake (mmol g^{-1})	CO_2/N_2 selectivity (IAST), 273 K[b]	CO_2/CH_4 selectivity (IAST), 273 K
T (K) =	273	298	323	Q_{st}[a] (kJ mol^{-1})	273	273	137	22 (5:95)
3D-mPOP	2.29	1.52	0.82	39.2	0.51	0.14		18 (50:50)

[a]Isosteric heats of adsorption (Q_{st}) values calculated using the gas adsorption data at 273, 298 and 323 K for CO_2 using the Clausius–Clapeyron equation. The Q_{st} value is reported at zero coverage.
[b]The IAST CO_2/N_2 selectivity was calculated based on the CO_2:N_2 ratio of 15:85 at 273 K.
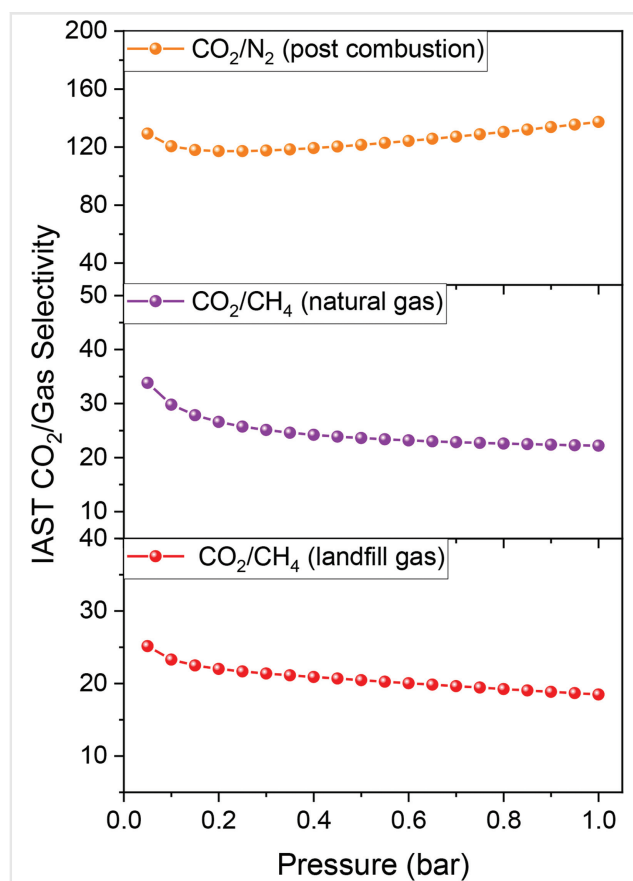
Figure 3 The IAST CO_2/N_2 and CO_2/CH_4 selectivities of the 3D-mPOP. The CO_2/N_2 selectivity was calculated using the gas ratio of CO_2:N_2 15:85 and CO_2:CH_4 5:95 (natural gas) and 50:50 (landfill gas).

towards CO_2, we decided to evaluate the CO_2 selectivity over N_2 and CH_4. The gas selectivity of 3D-mPOP was investigated by measuring the corresponding gas uptake isotherms at 273 K up to 1 bar. The initial steep increase in the case of CO_2 (Figure 2c) is attributed to the high affinity of the macrocyclic units for this guests. High CO_2 uptake at low partial pressures ($P/P_0 = 0.15$) is highly relevant, especially for flue gas separation. In order to calculate the mixed gas selectivity from single-component gas adsorption isotherms, we used the ideal adsorbed solution theory

(IAST), which is quite useful to evaluate the mixed gas selectivity for various porous materials.

3D-mPOP showed an excellent CO_2/N_2 (15:85) IAST selectivity of 137 under flue gas conditions at 1 bar. We also evaluated the performance of 3D-mPOP for natural gas (CO_2:CH_4, 5:95) and land fill gas (CO_2:CH_4, 50:50) separation (for performance comparison, see Table S2).[23] The IAST CO_2/CH_4 selectivities of 3D-mPOP for natural gas and land fill gas turned out to be 22 and 18, respectively (Figure 3) at 273 K, 1 bar. These values are significantly higher compared to the pillar[5]arene-based polymers[8a] and comparable to the POPs incorporating highly CO_2-philic organic cages.[5a] Moreover, 3D-mPOP also performed better than representative POPs such as BILPs[3c,24] and azo-COPs[25] thus clearly demonstrating the impact of the macrocycle (for a detailed comparison, see Table S2). High CO_2 selectivity of the 3D-mPOP over N_2 and CH_4 is attributed to the strong affinity of the macrocycle towards the linear guest molecules as well as to the larger kinetic diameter of N_2 (3.64 Å) and CH_4 (3.80 Å) compared to CO_2 (3.30 Å). These values clearly demonstrate the potential of 3D-mPOP for CO_2 removal from landfill gas and natural gas mixtures as well as CO_2 scrubbing.

Conclusions

We demonstrated the potential of cyclotetrabenzil as a functional organic building block to form fully sp^2-hybridized 3D polymer networks. Moreover, the high apparent affinity of the cyclotetrabenzil host towards the linear guest molecules was successfully transferred to the polymer network to achieve highly efficient CO_2 capture, with high selectivity over N_2 and CH_4. This study also underlines the potential of macrocycles and cages as building blocks for the synthesis of POPs for complex separations thanks to their highly selective host–guest interactions.

Experimental Section

All the chemicals and solvents were used as purchased without any further purification. Dry solvents were

purchased from Sigma-Aldrich or Acros Chemicals. The NaCl (99.95%) and KCl (99.95%) were purchased from Carl-Roth. The $ZnCl_2$ (99.995 trace metal basis), TABH (98%), and 1,2-phenylenediamine (98%) were purchased from Sigma-Aldrich. The hydrochloric acid solution (36.5%) was purchased from Honeywell Chemicals. All manipulations involving water and air-sensitive chemicals were carried in a glovebox under an argon atmosphere. The degassing and reactions under inert atmosphere were carried out using standard Schlenk line techniques. Silica gel chromatography was performed on 230–400 mesh silica gel (Silicyl). Thin layer chromatography was performed using Merck 60 F_{254} silica/alumina gel plates. FTIR spectra were recorded on a PerkinElmer Frontier spectrometer equipped with PIKe GladiATR module. The solution-phase NMR spectra were recorded using a Bruker Avance III 500 MHz spectrometer using deuterated solvents. The solid-state CP MAS ^{13}C NMR spectrum was recorded using a Bruker Avance Neo 400 MHz spectrometer using 7 kHz spinning rate and with a 5.0 s relaxation delay. The NMR spectra were calibrated based on the deuterated solvent peak. The XRD patterns were obtained using a STOE STADI-P system using Cu Kα1 incident beam. The samples were scanned between 2° and 60° of 2θ. The XPS measurements were carried out using a PHI VersaProbe II scanning XPS microprobe (Physical Instruments AG, Germany). Analysis was performed using a monochromatic Al Kα X-ray source of 24.8 W power with a beam size of 100 μm. The spherical capacitor analyzer was set at 45° take-off angle with respect to the sample surface. The pass energy was 46.95 eV yielding a full-width at half-maximum of 0.91 eV for the Ag 3d 5/2 peak. Curve fitting was performed using the fityk software. The EA was performed on a ThermoFischer Flash 2000 analyzer using BBOT as a reference standard. TGA was performed on a Mettler-Toledo TGA/DSC 3+ instrument using standard 70 μL alumina and 40 μL aluminium crucibles. The flow rate of the respective gas (air or N_2) was set to 20 sccm and the heating rate was set to 3 K/min. Nitrogen, CH_4 and CO_2 sorption was measured at 77 and 273 K using Micromeritics 3Flex instrument, after evacuation of the samples at 363 K for 24 h. The pore size distribution was determined via NLDFT. The field emission SEM images were obtained on a ThermoFischer Scios 2-focused ion beam scanning electron microscope using 3.0 kV accelerating voltage and 0.40 nA of current. The samples were coated with 5.0 nm gold using a Cressington 208HR sputter coater in order to avoid charging.

Procedures

The octaketone was prepared according to the previously reported literature procedure.[13–15] The 3D-mPOP was synthesized by the ionothermal method using a eutectic salt mixture composed of NaCl, KCl, and $ZnCl_2$ salts.[16] The mixture of 79.3 mg of octaketone (0.15 mmol), 85.2 mg of TABH (0.30 mmol), 18.4 mg of NaCl (0.315 mmol), 59.3 mg of KCl (0.795 mmol), and 169.7 mg of $ZnCl_2$ (1.245 mmol) was finely ground in a mortar. The resulting solid mixture was then transferred into a Pyrex ampule (18 mL) and evacuated under vacuum for 45 min before being flame-sealed. The ampule was heated in an oven at 250 °C for 48 h. After the completion of the polymerization, the contents of the ampule were washed with acetone (100 mL), THF (100 mL), methanol (100 mL), and water, respectively. Finally, the polymer was stirred in 500 mL of a 0.1M HCl solution for 5 d at RT before subsequent purification by Soxhlet extraction using methanol to yield 65.6 mg (66.2%) of 3D-mPOP as a black powder.

The *model compound* was synthesized using the same procedure in 85% yield as a brown powder.[14]

^1H NMR (CDCl$_3$, 500 MHz): δ 8.18 (dd, J = 5.8, 3.2 Hz, 8 H), 7.79 (dd, J = 5.8, 3.2 Hz, 8 H), 7.59 (s, 16H) ppm.

^{13}C NMR (CDCl$_3$, 125 MHz): δ 152.40, 141.62, 139.36, 130.65, 130.35, 129.53 ppm.

Funding Information

Supporting Information

Supporting Information for this article is available online at https://doi.org/10.1055/a-1512-5753.

Primary Data

Crystal structure data for octaketone have been deposited with the Cambridge Crystallographic Data Centre under code CCDC-2069402.

References

(1) Nandi, M.; Uyama, H. *Chem. Rec.* **2014**, *14*, 1134.

(2) Wang, W.; Zhou, M.; Yuan, D. *J. Mater. Chem. A* **2017**, *5*, 1334.

(3) (a) Patel, H. A.; Karadas, F.; Canlier, A.; Park, J.; Deniz, E.; Jung, Y.; Atilhan, M.; Yavuz, C. T. *J. Mater. Chem.* **2012**, *22*, 8431. (b) Jin, Y.; Voss, B. A.; Jin, A.; Long, H.; Noble, R. D.; Zhang, W. *J. Am. Chem. Soc.* **2011**, *133*, 6650. (c) Rabbani, M. G.; Reich, T. E.; Kassab, R. M.; Jackson, K. T.; El-Kaderi, H. M. *Chem. Commun.* **2012**, *48*, 1141. (d) Patel, H. A.; Je, S. H.; Park, J.; Chen, D. P.; Jung, Y.; Yavuz, C. T.; Coskun, A. *Nat. Commun.* **2013**, *4*, 1357. (e) Dawson, R.;

Adams, D. J.; Cooper, A. I. *Chem. Sci.* **2011**, *2*, 1173. (f) Jin, Y.; Voss, B. A.; McCaffrey, R.; Baggett, C. T.; Noble, R. D.; Zhang, W. *Chem. Sci.* **2012**, *3*, 874.

(4) D'Alessandro, D. M.; Smit, B.; Long, J. R. *Angew. Chem. Int. Ed.* **2010**, *49*, 6058.

(5) (a) Buyukcakir, O.; Seo, Y.; Coskun, A. *Chem. Mater.* **2015**, *27*, 4149. (b) Pederson, A. M.-P.; Gibson, H. W.; Slebodnick, C. *Supramol. Chem.* **2020**, *32*, 452. (c) Romano, V. J.; Macartney, D. H. *Supramol. Chem.* **2018**, *31*, 172.

(6) (a) Byun, Y.; Je, S. H.; Talapaneni, S. N.; Coskun, A. *Chem. Eur. J.* **2019**, *25*, 10262. (b) Byun, Y.; Coskun, A. *Angew. Chem. Int. Ed.* **2018**, *57*, 3173. (c) Chavez, A. D.; Smith, B. J.; Smith, M. K.; Beaucage, P. A.; Northrop, B. H.; Dichtel, W. R. *Chem. Mater.* **2016**, *28*, 4884.

(7) (a) Lu, W.; Yuan, D.; Zhao, D.; Schilling, C. I.; Plietzsch, O.; Muller, T.; Bräse, S.; Guenther, J.; Blümel, J.; Krishna, R.; Li, Z.; Zhou, H.-C. *Chem. Mater.* **2010**, *22*, 5964. (b) Charles, C. D.; Bloch, E. D. *Supramol. Chem.* **2019**, *31*, 508.

(8) (a) Dai, D.; Yang, J.; Zou, Y.-C.; Wu, J.-R.; Tan, L.-L.; Wang, Y.; Li, B.; Lu, T.; Wang, B.; Yang, Y.-W. *Angew. Chem. Int. Ed.* **2021**, *60*, 2. (b) Li, G.; Zhang, B.; Yan, J.; Wang, Z. *Chem. Commun.* **2016**, *52*, 1143. (c) Skorjanc, T.; Shetty, D.; Trabolsi, A. *Chem* **2021**, *7*, 882. (d) Shetty, D.; Jahović, I.; Skorjanc, T.; Erkal, T. S.; Ali, L.; Raya, J.; Asfari, Z.; Olson, M. A.; Kirmizialtin, S.; Yazaydin, A. O.; Trabolsi, A. *ACS Appl. Mater. Interfaces* **2020**, *12*, 43160. (e) Byun, Y.; Xie, L. S.; Fritz, P.; Ashirov, T.; Dincă, M.; Coskun, A. *Angew. Chem. Int. Ed.* **2020**, *59*, 15166. (f) Delente, J. M.; Umadevi, D.; Byrne, K.; Schmitt, W.; Watson, G. W.; Gunnlaugsson, T.; Shanmugaraju, S. *Supramol. Chem.* **2020**, *32*, 508.

(9) (a) Zhou, T.; Zhao, Y.; Choi, J. W.; Coskun, A. *Angew. Chem. Int. Ed.* **2019**, *58*, 16795. (b) Kim, J.; Elabd, A.; Chung, S.-Y.; Coskun, A.; Choi, J. W. *Chem. Mater.* **2020**, *32*, 4185.

(10) (a) Talapaneni, S. N.; Kim, D.; Barin, G.; Buyukcakir, O.; Je, S. H.; Coskun, A. *Chem. Mater.* **2016**, *28*, 4460. (b) Chen, X.; Wu, L.; Yang, H.; Qin, Y.; Ma, X.; Li, N. *Angew. Chem. Int. Ed.* **2021**, *60*, 1.

(11) McHale, C. M.; Stegemoller, C. R.; Hashim, M. I.; Wang, X.; Miljanić, O. Š. *Cryst. Growth Des.* **2019**, *19*, 562.

(12) Eisterhold, A. M.; Puangsamlee, T.; Otterbach, S.; Bräse, S.; Weis, P.; Wang, X.; Kutonova, K. V.; Miljanić, O. Š. *Org. Lett.* **2021**, *23*, 781.

(13) Wang, Y.-T.; McHale, C.; Wang, X.; Chang, C.-K.; Chuang, Y.-C.; Kaveevivitchai, W.; Miljanić, O. Š.; Chen, T.-H. *Angew. Chem. Int. Ed.* **2021**, in press; Doi: 10.1002/ange.202102813.

(14) Hahn, S.; Alrayyani, M.; Sontheim, A.; Wang, X.; Rominger, F.; Miljanić, O. Š.; Bunz, U. H. F. *Chem. Eur. J.* **2017**, *23*, 10543.

(15) (a) Alrayyani, M.; Miljanić, O. Š. *Chem. Commun.* **2018**, *54*, 11989. (b) Ji, Q.; Le, H. T. M.; Wang, X.; Chen, Y.-S.; Makarenko, T.; Jacobson, A. J.; Miljanić, O. Š. *Chem. Eur. J.* **2015**, *21*, 17205.

(16) Maschita, J.; Banerjee, T.; Savasci, G.; Haase, F.; Ochsenfeld, C.; Lotsch, B. V. *Angew. Chem. Int. Ed.* **2020**, *59*, 15750.

(17) Larkin, P. Infrared and Raman Spectroscopy: Principles and Spectral Interpretation. Elsevier Science: Amsterdam, **2011**.

(18) Mao, M.; Luo, C.; Pollard, T. P.; Hou, S.; Gao, T.; Fan, X.; Cui, C.; Yue, J.; Tong, Y.; Yang, G.; Deng, T.; Zhang, M.; Ma, J.; Suo, L.; Borodin, O.; Wang, C. *Angew. Chem. Int. Ed.* **2019**, *58*, 17820.

(19) Briggs, D. Handbook of X-ray Photoelectron Spectroscopy. Perkin-Elmer Corp. Physical Electronics Division: Minnesota, **1981**.

(20) Brunauer, S.; Emmett, P. H.; Teller, E. *J. Am. Chem. Soc.* **1938**, *60*, 309.

(21) Wang, P.; Zhang, G.; Chen, W.; Chen, Q.; Jiao, H.; Liu, L.; Wang, X.; Deng, X. *ACS Omega* **2020**, *5*, 23460.

(22) (a) Bardestani, R.; Patience, G. S.; Kaliaguine, S. *Can. J. Chem. Eng.* **2019**, *97*, 2781. (b) Thommes, M. *Chem. Ing. Tech.* **2010**, *82*, 1059.

(23) Othman, M.; Tan, S.; Bhatia, S. *Microporous Mesoporous Mater.* **2009**, *121*, 13.

(24) Sekizkardes, A. K.; Culp, J. T.; Islamoglu, T.; Marti, A.; Hopkinson, D.; Myers, C.; El-Kaderi, H. M.; Nulwala, H. B. *Chem. Commun.* **2015**, *51*, 13393.

(25) Buyukcakir, O.; Je, S. H.; Park, J.; Patel, H. A.; Jung, Y.; Yavuz, C. T.; Coskun, A. *Chem. Eur. J.* **2015**, *21*, 15320.